Characterizing underwater noise during rain at the northeast Pacific continental margin

Felix Schwock, and Shima Abadi

Citation: The Journal of the Acoustical Society of America **149**, 4579 (2021); doi: 10.1121/10.0005440
View online: https://doi.org/10.1121/10.0005440
View Table of Contents: https://asa.scitation.org/toc/jas/149/6
Published by the Acoustical Society of America

JASA ARTICLE

Characterizing underwater noise during rain at the northeast Pacific continental margin

Felix Schwock[a] and Shima Abadi[b]
Department of Electrical and Computer Engineering, University of Washington, Seattle, Washington, 98195, USA

ABSTRACT:
Large scale studies of underwater noise during rain are important for assessing the ocean environment and enabling remote sensing of rain rates over the open ocean. In this study, approximately 3.5 yrs of acoustical and meteorological data recorded at the northeast Pacific continental margin are evaluated. The acoustic data are recorded at a sampling rate of 64 kHz and depths of 81 and 581 m at the continental shelf and slope, respectively. Rain rates and wind speeds are provided by surface buoys located in the vicinity of each hydrophone. Average power spectra have been computed for different rain rates and wind speeds, and linear and nonlinear regression have been performed. The main findings are (1) the linear regression slopes highly depends on the frequency range, rain rate, wind speed, and measurement depth; (2) noise levels during rain between 200 Hz and 10 kHz significantly increase with increasing wind speed; and (3) the highest correlation between the spectral level and rain rate occurs at 13 kHz, thus, coinciding with the spectral peak due to small raindrops. The results of this study indicate that previously proposed algorithms for estimating rain rates from acoustic data are not universally applicable but rather have to be adapted for different locations.
 https://doi.org/10.1121/10.0005440
(Received 19 November 2020; revised 2 June 2021; accepted 4 June 2021; published online 28 June 2021)
[Editor: D. Benjamin Reeder] Pages: 4579–4595

I. INTRODUCTION

Ocean ambient noise reveals important information about marine life, natural phenomena, and the human footprint in the ocean. The general spectrum characteristics of the ambient noise are described by the Wenz curves (Wenz, 1962). Observations by Wenz (1962) have shown that rain and wind are important sources of underwater ambient noise for frequencies above 100 Hz. Early studies in water tanks (Franz, 1959; Nystuen, 1986) have identified two important sound generating mechanisms when droplets strike the water surface: (1) the impact of the droplet on the surface generating a broadband white noise spectrum in which the spectral level is highly dependent on drop radius and impact velocity; and (2) an oscillating air bubble emerging during the drop impact and radiating acoustic energy between 1 and 20 kHz. The sound from the oscillating air bubble is particularly significant during light rain and drizzle when a broad spectral peak around 15 kHz can be observed. Several measurements conducted in lakes have shown that the underwater noise spectrum generated by actual rain is in good agreement with these laboratory studies and especially the broadband peak around 15 kHz was confirmed (Bom, 1969; Laville *et al.*, 1991; Nystuen, 1986; Scrimger *et al.*, 1987).

The dependence of the impact and bubble sound on the drop diameter D was further analyzed in a series of papers and can be summarized as follows: (1) Small raindrops ($0.8\,\text{mm} \leq D < 1.1\,\text{mm}$) produce a broadband impact sound, followed by a much louder sound caused by the damped oscillation of microbubbles, called *type I* microbubbles, at frequencies centered around 15 kHz (Medwin *et al.*, 1992). The emergence of *type I* microbubbles, however, is highly wind dependent (Medwin *et al.*, 1990) and quickly decreases if the incident angle of the rain drop deviates from normal. (2) Medium size raindrops ($1.1\,\text{mm} \leq D < 2.2\,\text{mm}$) are particularly quiet and do not create bubbles, thus, only contributing a little to the underwater soundscape (Nystuen, 2001). (3) Large raindrops ($D > 2.2\,\text{mm}$) produce a loud impact sound (Medwin *et al.*, 1992; Pumphrey *et al.*, 1989). Furthermore, two types of bubbles, which radiate similar acoustic sound energy, can be observed. The first type (*type II* microbubbles) is a direct result of the drop impact and largely contributes to the sound spectrum below 10 kHz (Medwin *et al.*, 1992). The second type (*type III* microbubbles) is caused by drop aerosols, which are generated during the initial impact and oscillate with frequencies typically between 3 and 25 kHz (Nystuen and Medwin, 1995).

These studies were complemented by open ocean measurements during light rain (Scrimger *et al.*, 1989) and heavy rain (Nystuen *et al.*, 1993). The latter showed that heavy rain results in an increase in the noise level over a frequency range of 4–21 kHz, and no spectral peak at 15 kHz

[a]Electronic mail: fschwock@uw.edu
[b]Also at: Division of Engineering and Mathematics, University of Washington, Bothell, WA 98011, USA.

can be observed. For very heavy rain with rain rates of 150 mm/h or higher, a decrease in the spectral level above 10 kHz was observed (Nystuen *et al.*, 1993). This phenomenon can be explained by a layer of bubbles forming below the water surface and attenuating sound in high frequency ranges.

Because wind is oftentimes present during rain events, the effect of wind noise on the spectral level has to be considered when analyzing the noise pattern generated by the rain. Several studies have shown that the spectral level of wind noise increases with increasing wind speed. Plotting the spectral levels in dB re 1 μPa^2/Hz versus the log frequency, a constant slope for frequencies above 1 kHz and wind speeds smaller than 15 m/s has been observed (Knudsen *et al.*, 1948; Lemon *et al.*, 1984; Ma *et al.*, 2005; Vagle *et al.*, 1990; Wenz, 1962). This slope is usually between -16 dB/decade (dB/dec) and -20 dB/dec and varies between different measurements and locations. For frequencies below 1 kHz, Wenz (1962) has shown that wind noise has a spectral peak between 100 Hz and 1 kHz. For very high wind speeds, a layer of bubbles resulting from increased surface agitation forms below the water surface, which results in a decrease in the spectral level at high frequencies (Farmer and Lemon, 1984), similar to the phenomenon observed for very high rainfall rates.

A much detailed analysis of the spectral shape of noise during rain for different rain rates and wind speeds, evaluating about 90 buoy months of data from several hydrophones located at the Western Pacific Warm Pool and the Inter-tropical Convergence Zone, was conducted by Ma *et al.* (2005). An important finding of this study is that the spectral sound level between 3 and 10 kHz for different rain rates is almost independent of the wind speed for wind speeds up to 14 m/s.

Whereas in all of the field studies discussed above, the hydrophones were deployed close to the surface (maximum depth of about 100 m), Anagnostou *et al.* (2008) and Barclay and Buckingham (2013) showed that the typical rain noise pattern can also be detected at greater depths.

In this study, acoustic data from two hydrophones located on the continental margin of the Eastern North Pacific are examined and power spectral density (PSD) estimates for different rain rates and wind speeds are evaluated over a range from 30 Hz to 25 kHz. The hydrophones are placed at two different depths in two different locations at the continental margin off the coast of Oregon. Surface buoys containing rain gauges and wind speed sensors are located in the vicinity of the hydrophones. As hydrophones and surface rain gauges used in this study are horizontally displaced, the rain rate measurements have been matched with the corresponding noise pattern before evaluating the data. The PSD estimates between these two locations are compared, and the depth dependence is analyzed.

The remainder of this paper is divided into five sections. Section II describes the experiment and the data acquisition system. Section III gives an overview of the acoustic environment. Section IV presents algorithms for detecting rain events, processing the acoustic data, and matching the rain rate measurements with the corresponding acoustic patterns. Section V discusses the results from our measurements by evaluating the PSD estimates for various rain rates and wind speeds. Section VI summarizes this research effort and states the conclusions drawn from it.

II. INSTRUMENTATION AND DATA COLLECTION

The acoustic and meteorological data used in this paper were recorded between December 2015 and June 2019 by the Coastal Endurance Array, which is maintained by the Ocean Observatories Initiative (OOI). The instruments are located at two sites that are approximately 59 km apart from each other as shown in Fig. 1(a). The first site is located at the continental slope at 44°22′8.4″ N and 124°57′14.4″ W. The instruments in this site are part of the Oregon Offshore Cabled Benthic Experiment Package[2] and Oregon Offshore Surface Mooring[3] of the OOI Coastal Endurance Array. The hydrophone is deployed on the sea floor at a depth of 581 m. This site is referred to as the *deep location* throughout this paper. The second site is located at the continental shelf at 44°38′13.2″ N and 124°18′21.6″ W. The instruments in this site are part of the Oregon Shelf Cabled Benthic Experiment Package[4] and Oregon Shelf Surface Mooring[5] of the OOI Coastal Endurance Array. The hydrophone is deployed on the sea floor at a depth of 81 m. This site is referred to as the *shallow location* throughout this paper. At each site, there is a surface buoy deployed close to the hydrophone, which is measuring rain accumulation and wind speed. The positions of the surface buoys relative to the hydrophones are shown in Fig. 1(b). The horizontal distance between the

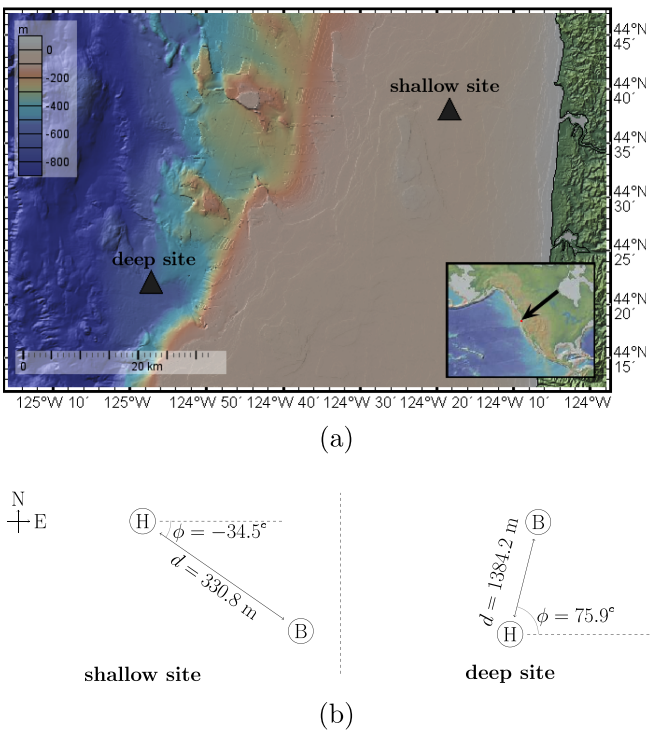

FIG. 1. (Color online) (a) Locations of the deep and shallow sites in the northeast Pacific Ocean [the figure was made with the GeoMapApp (footnote 1); Ryan *et al.*, 2009) and (b) displacements of hydrophone (*H*) and surface buoy (*B*) at each location.

https://doi.org/10.1121/10.0005440

hydrophone and surface buoy is 330.8 m at the shallow location and 1384.2 m at the deep location.

A. Acoustic data collection

Acoustic data are recorded by broadband icListen HF hydrophones (Ocean Sonics, Nova Scotia, Canada) with sensitivity −169 dB re 1 V/μPa. The raw acoustic data are accessible on the data server of the OOI. The calibration data are available by Ocean Sonics for the icListen HF instruments at a depth of 1 m and frequency ranges of 0–200 kHz, observed during the experiment in a water tank. The frequency range of the hydrophones is roughly 10 Hz–200 kHz The hydrophones record continuously at a sampling rate of 64 kHz and transmit the acoustic data to the shore via a fiber-optic cable.

B. Meteorological data collection

Meteorological measurements are provided by surface buoys located in the vicinity of each hydrophone. The cumulative rain and wind speed samples are acquired every 30–65 s (on average every 60 s), transmitted to the shore via a satellite link, and accessible on the data server of the OOI.

The rain accumulations are measured by an *RM Young 50202* (Traverse City, MI) self-siphoning capacitance rain gauge with a cylindrical catchment area of 100 cm^2 and a volume of 500 ml. Thus, the cumulative amount of rain is measured in a range of 0–50 mm with a nominal precision of 1 mm. When the catchment basin of the rain gauge is full, water is automatically released via a drain. These siphoning events usually last for about 30 s (Nystuen, 1996). To compute the rain rates, the difference in the rain amount between two consecutive samples is divided by the time difference between those samples. Due to the relative small catchment area of the rain gauge, 1-min rain rate measurements are prone to errors from isolated drips typically occurring during light rain (Nystuen, 1999; Nystuen *et al.*, 1996). These drips can cause peaks in the rain rate and, thus, overestime its actual value. The analysis by Nystuen *et al.* (1996) estimates that the mean relative error of 1-min rain rate samples of *RM Young* capacitance rain gauges is about ±38%–40% for rain rates below 5 mm/h and ±12%–14% for rain rates above 5 mm/h. Furthermore, the measurement precision decreases at high wind speeds (in the study by Nystuen, 1999, a wind speed of 4.1 m/s) due to heavier movement of the water in the catchment basin.

The wind speeds are measured by a *Gill Windobserver II* (Hampshire, UK) wind speed sensor, which measures the northward and eastward wind component in m/s with a nominal precision of 2% and 1 deg. The wind speed values are smoothed using a sliding 21-point symmetric Hann window to reduce the measurement variance.

III. DESCRIPTION OF ACOUSTIC ENVIRONMENT

A. Sound propagation conditions

Conductivity, temperature, and depth sensors (CTDs) collocated with the hydrophones are used to compute sound speed profiles for the deep and shallow locations according to Eqs. (3)–(5) in Chen and Millero (1977). Multiple CTDs are operating at different depth at each location, and the data are combined to obtain sound speed profiles over the entire water column. Both locations have a CTD connected to the surface buoy (7 m depth), a shallow profiler CTD moving up and down the water column (between 20 and 200 m for the deep and 0–80 m for the shallow location), and a bottomed CTD at the hydrophone. Additionally, the deep location has a deep profiler CTD (175–500 m; was only operating a few times during the measurement period) and a CTD at a 200 m platform. The CTD data can also be downloaded from the OOI servers.[6]

Typical summer and winter sound speed profiles for both locations are shown in Fig. 2. During summer (July and August), the sound speed is downward refracting at both locations with a near surface duct between 0 and 100 m, observable at the deep location. In contrast to that, the sound speed profiles during winter (December and February) show less variability over the water column. Especially at the shallow location, the speed of sound is almost constant during December. Note that the dashed line in the February data indicates that the deep profiler was not operating and, thus, no CTD data are available between 200 and 580 m. The variations in the sound speeds between summer and winter months indicate that the propagation pattern varies seasonally.

Anagnostou *et al.* (2008) have shown that hydrophones have an effective surface listening area that can be defined as the area generating 90% of the acoustic energy received by the hydrophone. This area generally decreases with increasing frequency and decreasing hydrophone depth, but also depends on the sound propagation conditions. Using their method, we have estimated the effective surface listening areas for the deep and shallow hydrophone for three acoustic frequencies (500 Hz, 5 kHz, and 15 kHz). The results are shown in Fig. 3. For both locations, the 90%

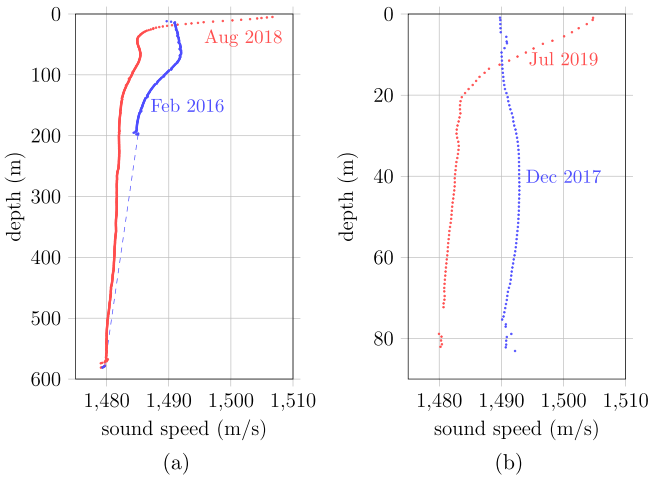

FIG. 2. (Color online) Typical summer and winter sound speed profiles for the (a) deep and (b) shallow locations. The dashed line in the February data at the deep location indicates that no deep profiler CTD data were available during this month.

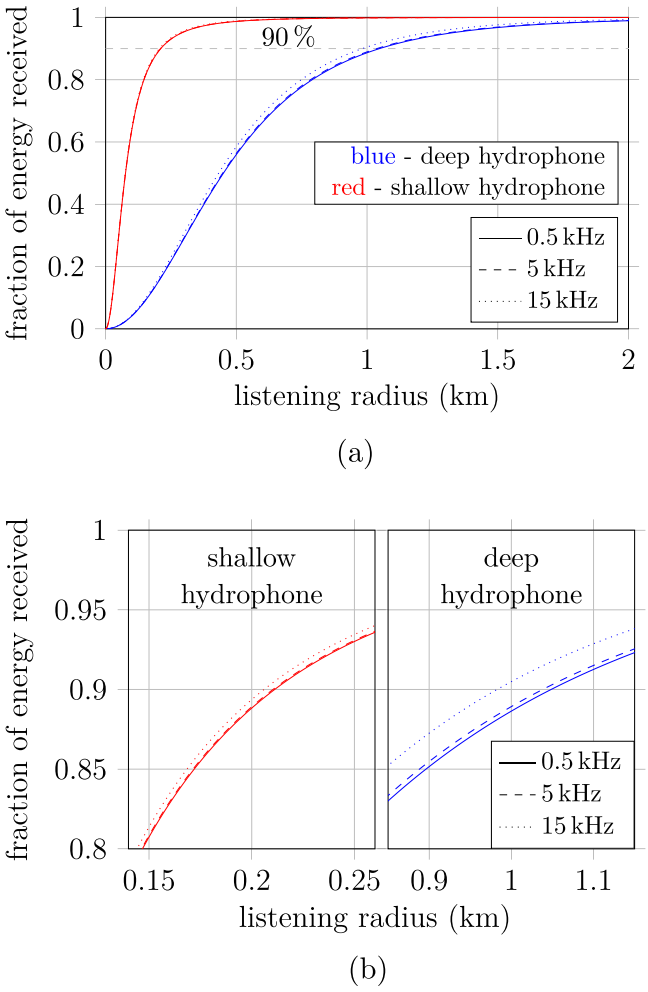

FIG. 3. (Color online) The fraction of surface energy received by the hydrophones as a function of the surface listening radius. The effective surface listening area can be defined as the area where 90% of the acoustic energy originates from [(a) full plot, (b) zoomed-in around the effective listening radius]. We assumed the following environmental parameters (which are averages over the months in Fig. 2) when computing the curves: deep location, pH = 8.1, temperature = 7.37 °C, and salinity = 33.86 ppt; shallow location, pH = 8.1, temperature = 10.03 °C, and salinity = 33.05 ppt.

effective listening area depends only weakly on the frequency and has a radius of about 1 km for the deep hydrophone (581 m depth) and 200 m for the shallow hydrophone (81 m depth). It turned out that seasonal variations in temperature, sound speed, and salinity have a negligible effect on the listening area.

The effective surface listening area effects the spatial averaging of noise. That is, a larger listening radius means that, for example, as a rain shower passes over the measurement location, the onset of rain can be detected earlier in the acoustic signal. Anagnostou *et al.* (2008) have shown that noise measured by a deep hydrophone (in their study, depths of 1 km and 2 km) and, hence, averaged over a larger surface area, shows better correlation with radar rain measurements averaged over a larger area than with rain measurements averaged over a small surface area. Noise during rain measured by a hydrophone deployed in 60 m depth, on the other hand, shows better correlation to rainfall averaged over a small area. As the rain rate in our study is measured by a single surface buoy and so no spatial averaging is performed, the correlation between the rain rate and underwater noise is, therefore, expected to be better at the shallow location.

B. Acoustic soundscape

The acoustic soundscape at both measurement sites is impacted by a variety of sources such as wind, rain, ships, marine mammals, and other measurement devices. Although Sec. IV B provides a method for removing and mitigating the effects of distortions from ships, marine mammals, and the measurement apparatus, wind is often present at the same time as rain and, thus, can contribute significantly to the underwater soundscape during rain. Indeed, the OOI dataset allows for a thorough analysis of wind-only noise (i.e., wind noise in the absence of rain and other noise sources). However, as this goes beyond the scope of this paper, we only give a brief summary here of the spectral characteristics of wind-only noise at the northeast Pacific continental margin.

It was found that wind noise spectral levels above 200 Hz decrease with increasing frequency. In a logarithmic frequency scale, spectral levels decrease linearly with different slopes in the 0.2–3 kHz and 3–25 kHz ranges. The slopes are, on average, greater in the higher frequency range and, in general, depend on the wind speed. Only at the shallow location above 3 kHz and for wind speeds below 10 m/s, slopes are independent of the wind speed with values between −13 and −14 dB/dec. Furthermore, we found that slopes at the deep location are greater than those at the shallow location. The results also show that spectral levels over the entire frequency range increase with increasing wind speed for both locations (with each doubling of the wind speed, spectral levels increase by 6–10 dB).

IV. DATA PROCESSING

A successful evaluation of underwater noise during rain requires careful processing of the measured data. This includes detecting rain events from the *RM Young* (Traverse City, MI) rain gauges, identifying the acoustic recordings at the time of those rain events, and estimating the spectral levels. In the following, we will elaborate those steps in more detail.

A. Rain event detection from RM Young rain gauges

The main challenge in automatically detecting rain events from the *RM Young* (Traverse City, MI) rain rate signal is the high variance of the 1-min rain rate samples. Following the approach described by Ma and Nystuen (2005), a 21-point Hann window is used as a moving average filter to reduce the variance of the rain rates and mitigate the effect of spikes. This process is illustrated in Fig. 4. One can see that the *RM Young* rain rate can fluctuate with values up to ±5 mm/h, whereas the averaged rain rate eliminates these fluctuations and only preserves a few distinct peaks. A rain event can now be defined as the collection of consecutive rain rate samples whose average rain rate exceeds a threshold of

https://doi.org/10.1121/10.0005440

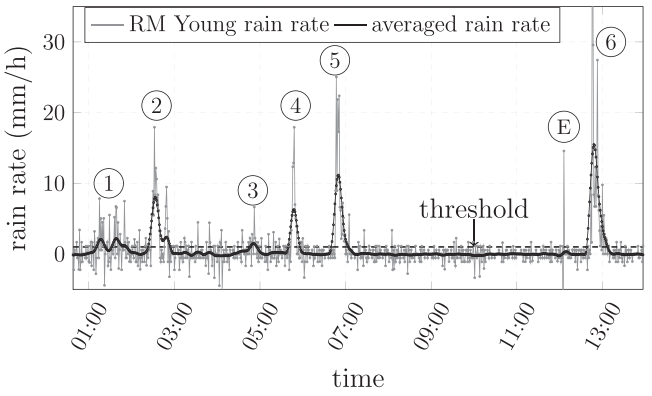

FIG. 4. Six rain events (circled numbers) during May 20, 2016 at the deep location. The gray and black lines show 1-min rain rate samples and the averaged rain rate using a 21-point Hann-window moving average filter, respectively. The averaged rain rate exhibits a significant reduction in the measurement noise and faulty spikes, such as point *E*, are removed. A rain event is defined as the collection of samples whose averaged rain rate exceeds 1 mm/h.

1 mm/h. Rain events that are separated by less than 10 min are considered as single rain events (e.g., event 1 in Fig. 4). Once the rain events are detected, the original 1-min rain rate samples (not the averaged rain rates) are used for the analysis. It is noted that only *RM Young* rain rates greater than 2 mm/h are considered in the analysis in Sec. V to avoid the use of negative rain rate samples, which occur especially at the onset and offset of rain events as a result of inaccuracies in the rain accumulation measurements.

B. Processing of acoustic data

PSDs are calculated using the Welch's overlapped segment averaging method (Welch, 1967), which is computationally efficient and, thus, suitable for handling large data sets. The Python package OOIPy (Schwock *et al.*, 2020) is used for these calculations. A Hann window was applied to 64 ms (4096 samples) data blocks with 32 ms overlaps (50%) to minimize the spectral leakage at the corners. Afterward, a frequency-wise median averaging as described and analyzed by Schwock and Abadi (2021) was applied to the 4096-point fast Fourier transforms of 1875 data blocks to produce sequential 1-min power spectrum levels over the duration of each rain event. It is noted that the actual number of data blocks varies between 937 and 2031 as the rain rate is measured in intervals between 30 and 65 s. A frequency dependent sensitivity correction using the calibration data of the hydrophones is applied to the PSD estimates.

The interference from acoustic Doppler current profilers (ADCPs) co-located with the hydrophones is removed by using a median averaging in the Welch's method instead of a mean averaging (Parks *et al.*, 2009; Schwock and Abadi, 2021). Furthermore, to solely focus on rain and wind noise, the acoustic data contaminated by other noises are manually flagged and removed from the analysis. To do so, spectrograms with a linear frequency scale from 0 to 32 kHz were first computed for each rain event and, next, manually inspected for the following types of distortions: (1) ship noise with a time-frequency pattern as described by McKenna *et al.* (2012), (2) broadband stationary interfering signals with a spectral level significantly above the background noise and often characterized by a sudden onset or offset, and (3) strong bioacoustic signatures in the low frequency region. The second type of distortion is thought to be caused by other oceanographic instruments and the motors of the water column profilers operating at each location. The percentage of spectrograms showing such types of distortions and, thus, being rejected from the analysis, is approximately 47% at the deep location and 54% at the shallow location.

Finally, it is noted that multiple narrow band tones, presumably caused by the measurement apparatus, can be observed in the acoustic signals. At the deep location, six strong tones approximately at 6.27, 8.34, 12.53, 14.03, 16.09, and 16.7 kHz were identified. At the shallow location, five tones approximately at 7.45, 11.17, 13.28, 15.31, and 19.38 kHz were identified. Those tones have been removed from all of the plots in Sec. V by linearly interpolating the spectral level over a range of approximately 190 Hz (12 samples) around each tone.

C. Offset correction

The spatial averaging of the acoustic signal due to the effective surface listening area, along with the horizontal displacement between hydrophones and surface buoys [see Fig. 1(b)], can cause an offset between the rain rate detected by the *RM Young* (Traverse City, MI) rain gauge and the corresponding noise pattern. To get an accurate estimate of the noise spectral level associated with different rain rates, this offset is to be estimated and, subsequently, eliminated for each rain event. To do so, we propose the following algorithm:

(1) Spectrograms for each rain event (10 min are added before and after each rain event to accurately capture the onset and offset of the event) are computed by dividing the entire noise signal during a rain event into K 1-s intervals, indexed by k, computing the spectral estimate $\hat{S}^{1s}(f,k)$ for the kth interval using the Welch's median method as described in Sec. IV B, and then concatenating all $\hat{S}^{1s}(f,k)$, where the index k ranges from $-\lfloor (K-1)/2 \rfloor$ to $\lfloor (K-1)/2 \rfloor$.

(2) The average noise power for each spectrogram is computed by

$$P_{\text{noise}}(k) = \frac{1}{N}\sum_{f} 10\log_{10}\left(\hat{S}^{1s}(f,k)\right), \tag{1}$$

where $N = 2049$ is the number of frequency bins between 0 and 32 kHz.

(3) The *RM Young* (Traverse City, MI) rain rate signal containing 1-min rain rate samples is interpolated using a univariate spline with a degree of smoothing of three to obtain a rain rate signal $\tilde{R}$, which is defined for the same time steps k as P_{noise}.

(4) The cross correlation $(\tilde{R} \star P_{\text{noise}})(k)$ between the interpolated rain rate and average noise power is computed.
(5) The offset between the rain rate and associated noise signals, in seconds, is defined as the index k corresponding to the maximum of the cross correlation,

$$\text{offset} = \arg\max_k (\tilde{R} \star P_{\text{noise}})(k). \tag{2}$$

Figure 5 shows spectrograms, P_{noise}, $\tilde{R}$, and $\tilde{R} \star P_{\text{noise}}$ for rain event 2 from Fig. 4. Note that the cross correlation in Fig. 5(c) is normalized by its value at lag zero. One can observe that as P_{noise} and $\tilde{R}$ have distinct peaks, the cross correlation function exhibits a distinct maximum with a high correlation value. As the entire noise power is expected to increase with increasing rain rate, rain events with a high maximum rain rate are expected to achieve higher correlation values compared to events exhibiting a lower maximum rain rate, thus, giving more reliable estimates of the offset. For rain events with lower rain rates and less structure in terms of $\tilde{R}$ and P_{noise}, the maximum correlation is often low, suggesting that the estimated offset is less likely to represent an actual shift between the rain rate and P_{noise}.

The average offset of all rain events is 195 s (standard deviation 290 s) at the shallow location and 235 s (standard deviation 513 s) at the deep location. This means that most rain events (approximately 62% at both locations) are first recorded at the hydrophone and afterward at the surface buoy. Attempts to correlate the offset with the wind direction have not revealed any significant relation.

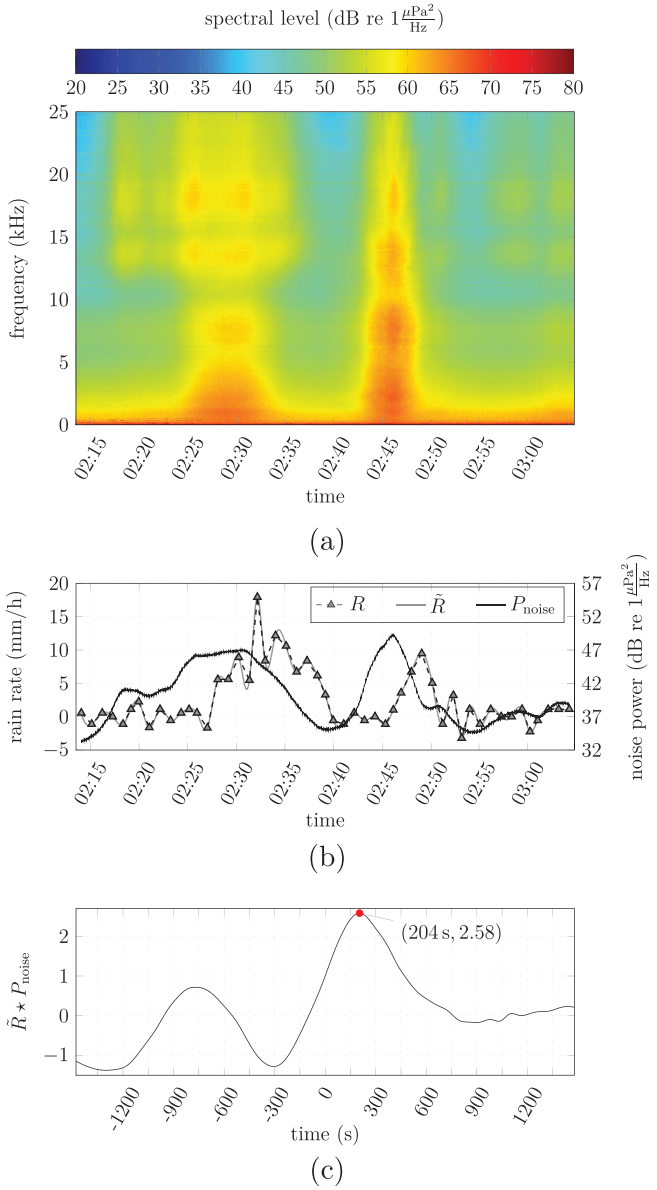

FIG. 5. (Color online) (a) The specrogram along with (b) the average noise power P_{noise}, 1-min rain signal R, and interpolated rain signal $\tilde{R}$, and (c) the cross-correlation function $\tilde{R} \star P_{\text{noise}}$ normalized by its value at lag zero for Event 2 shown in Fig. 4. The offset corresponds to the maximum of the cross correlation: $\arg\max_k(\tilde{R} \star P_{\text{noise}})(k)$. If $\tilde{R}$ and P_{noise} exhibit distinct peaks with high values, $\tilde{R} \star P_{\text{noise}}$ also shows a distinct maximum.

V. CHARACTERIZING NOISE DURING RAIN

In this section, the power spectrum estimates of noise during rain along the northeast Pacific Ocean continental margin are presented and discussed. Results using data collected at two depths will be compared to analyze the depth dependency of the noise. The influence of the rain rate and wind speed on the spectral levels is highlighted and compared to the results from previous studies.

In this study, the rain rate and wind speed categories are adopted from Ma *et al.* (2005). The rain events are detected as described in Sec. IV A and inspected for interfering signals as described in Sec. IV B. For the remaining valid rain events, the offset between the acoustic data and rain rate measurements is computed and eliminated using the algorithm presented in Sec. IV C. Rain events that last less than 3 min or have an offset greater than 10 min are discarded. In total, 212 rain events at the deep location and 443 rain events at the shallow location, which range in length between 3 and 286 min with a median around 15 min, are considered for the analysis. The distribution of the rain events over the measurement period is shown in Fig. 6. The difference in the distribution between the deep and shallow sites is mainly caused by differences in data availability as well as different distributions of the acoustic distortions at each location.

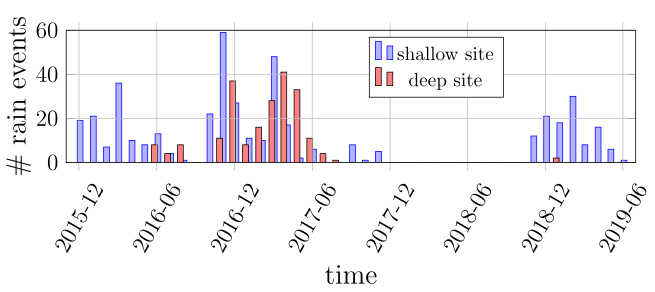

FIG. 6. (Color online) Distribution of rain events between December 2015 and June 2019 at the deep and shallow locations, which are considered for the analysis of noise during rain.

https://doi.org/10.1121/10.0005440

TABLE I. Number of PSD samples for the average spectra shown in Fig. 7.

	Rain rate (mm/h)											
	Deep hydrophone						Shallow hydrophone					
Wind speed (m/s)	<2	2–5	5-10	10–20	20–30	30–50	<2	2–5	5–10	10–20	20–30	30–50
0–2	62	58	37	8	3	—	190	86	47	13	—	2
2–4	234	133	68	15	—	—	570	342	154	38	9	3
4–6	626	378	179	29	2	1	1280	822	328	109	31	13
6–8	506	340	160	42	5	6	1673	1032	411	115	11	13
8–10	500	332	132	19	—	3	1076	714	322	59	10	5
10–12	383	209	75	18	1	2	687	467	170	34	2	5
12–14	152	72	35	5	—	—	259	171	82	21	2	1
>14	199	138	44	6	1	—	157	109	49	7	1	—

Each rain event consists of multiple rain rate and wind speed samples. A PSD sample is calculated for each rain rate and wind speed as described in Sec. IV B. Only rain rates above 2 mm/h are considered in the subsequent analysis. The numbers of PSD samples calculated in each category are listed in Table I. Because there are only a few PSD samples available for rain rates above 20 mm/h, the results in those categories should be regarded with greater caution.

Figure 7 shows the average PSDs for the different rain rate and wind speed categories. Furthermore, the standard deviation for each category is illustrated by the shaded area around each average PSD (for a better representation, only one-quarter of the standard deviation is plotted). Figure 7 shows that the power spectra for each rain rate category significantly depend on the wind speed, particularly at frequencies above 100 Hz. The difference in the spectral level between the lowest and highest wind speed usually exceeds 15 dB between 500 Hz and 5 kHz at both locations, which is in contrast to the results reported by Ma *et al.* (2005), who found that noise spectral levels during rain in the tropical Pacific Ocean are almost independent of the prevailing wind speed for frequencies between 1 and 10 kHz. This can likely be attributed to the different measurement locations and depths and, therefore, differences in the sound propagation properties and effective surface listening areas (most of Ma's hydrophones were deployed in a depth of 38 m, whereas our hydrophones are deployed on the sea floor at depths of 81 m and 581 m, respectively). It also implies that noise spectral levels during rain cannot be generalized across different locations. The variance of the PSD estimates within each rain rate and wind speed category (shaded area) is likely a result of the variability of the noise levels as well as the variance of the rain rate and wind speed measurements itself. Rain rates below 5 mm/h, especially, are subjected to larger errors as shown in Sec. II B. This can potentially result in more misassignments of the corresponding PSD estimates to their respective rain rate categories and, thus, an increased variance of the noise spectral levels. However, as there are multiple mechanisms driving the variance of the PSD estimates and only a few samples are available for higher rain rate categories, no definite conclusions about the variance of the noise levels can be drawn at this point.

To further analyze the spectral characteristic of noise during rain, we have divided the spectra into four frequency ranges: 30–200 Hz (very low frequency range), 0.2–1 kHz (low frequency range), 1–10 kHz (medium frequency range), and 10–25 kHz (high frequency range). Frequencies below 30 Hz and above 25 kHz are filtered out and, hence, excluded from the analysis.

A. Very low frequency range (30–200 Hz)

This frequency range exhibits the greatest difference between the deep and shallow locations. Spectral levels measured by the deep hydrophone are often 10–12 dB higher compared to the shallow location. Furthermore, deep hydrophone spectral levels around 50 Hz are significantly higher than at other frequencies, especially for low and moderate wind speeds. This pattern is not observed in the spectral levels measured by the shallow hydrophone except for low wind speeds and light and moderate rain (wind speed smaller than 2 m/s and rain rates smaller than 20 mm/h). A similar phenomenon was also reported in other studies, such as Berger *et al.* (2018), Farrokhrooz *et al.* (2017), and is likely caused by noise from distant ships (Anderson, 1979; Wagstaff, 1981; Wenz, 1962) and high latitude winds (Bannister, 1986) that propagate in the deep sound channel. As the acoustic environment at the shallow location is dominated by steep bottom and surface reflections, the influence of distant sources is negligible, and no increased spectral levels at very low frequencies can be observed. Because frequencies between 30 and 200 Hz are not dominated by rain events in proximity to the hydrophones, this frequency range is not further regarded in the characterization of ambient noise during rain.

It shall be noted that an anomalous, sharp peak can be observed for the deep hydrophone in the 20–30 mm/h rain rate and 0–2 m/s wind speed category. Unfortunately, there are not enough samples in this category to find the origin of this peak (only three samples are available). We assume that malfunctioning devices in the experimental package are responsible for these distortions.

B. Low frequency range (0.2–1 kHz)

In the frequency range between 0.2 and 1 kHz, noise during rain significantly depends on the wind speed.

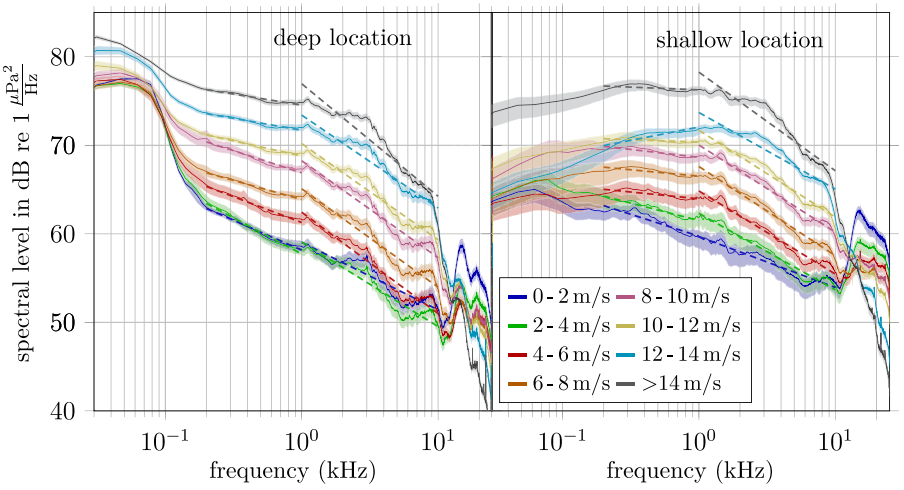

(a) rain rate: 2 - 5 mm/h

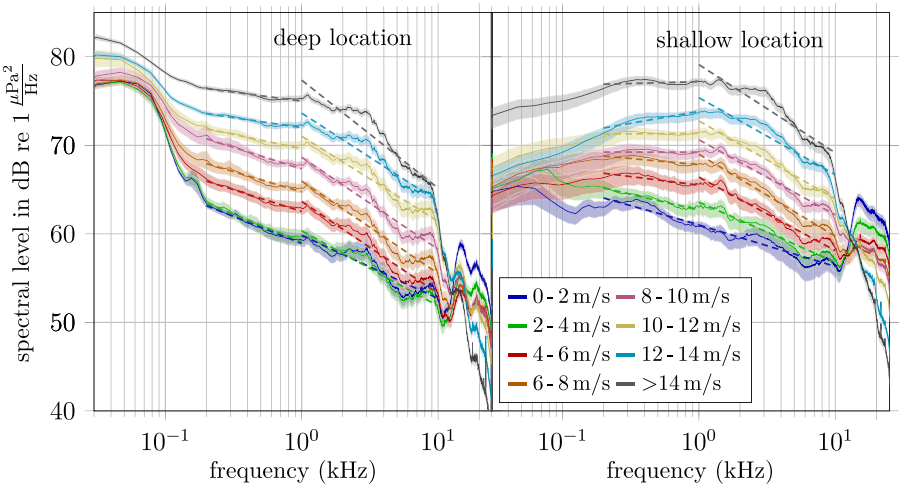

(b) rain rate: 5 - 10 mm/h

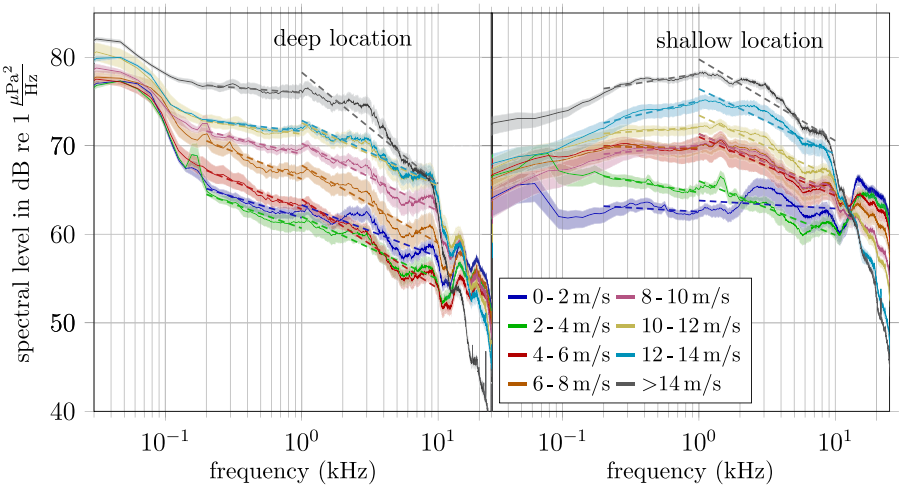

(c) rain rate: 10 - 20 mm/h

FIG. 7. (Color online) Average PSD estimates of noise during rain for various rain rate categories. The shaded areas around each average PSD mark one-quarter of the standard deviation. The linear regression results in the low and medium frequency range are shown as dashed lines. The number of PSD samples for each rain rate and wind speed category is given in Table I. Because there are only a few PSD samples available for rain rates above 20 mm/h, the average PSDs in those categories should be regarded with greater caution. Slopes and R^2 scores of the linear regression are provided in Figs. 8 and 9. A strong wind speed dependence of the noise spectral levels for frequencies above 100 Hz can be observed at both locations.

https://doi.org/10.1121/10.0005440

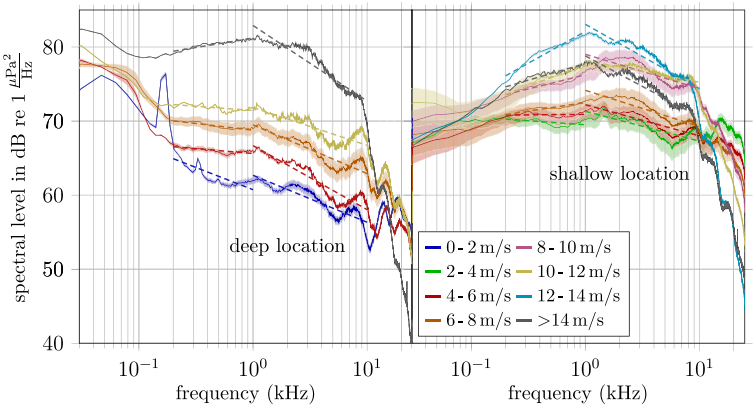

(d) rain rate: 20 - 30 mm/h

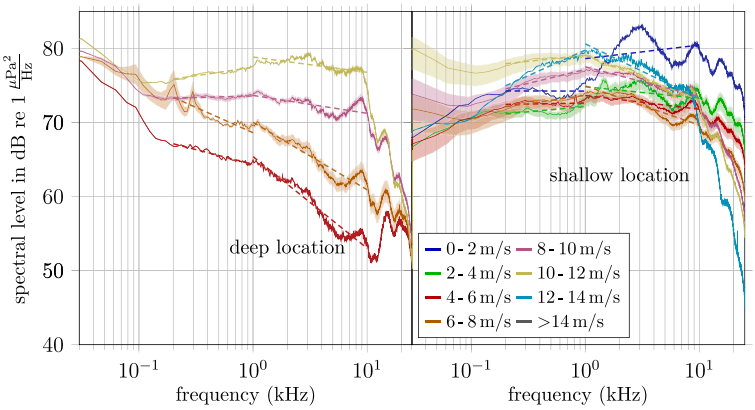

(e) rain rate: 30 - 50 mm/h

FIG. 7. (*Continued.*)

Specifically, for rain rates below 10 mm/s, the spectral level monotonically increases, typically by 1–3 dB, with increasing wind speeds at both locations. For rain rates above 10 mm/h, this pattern can still be observed, although it is less distinct as average PSDs are usually comprised of fewer PSD samples and, thus, are less likely to represent the true spectral levels for these categories.

It is interesting to note that the spectral level in the 0–2 m/s wind speed category is almost identical to the spectral level in the 2–4 m/s category, especially at the deep location and for rain rates below 10 mm/h. A possible explanation is that breaking waves and whitecaps, which are important sound generating mechanisms (Kerman, 1984), are not emerging for wind speeds below approximately 3 m/s (Monahan, 1971; Monahan and Lu, 1990). That is, for wind speeds below 3 m/s, the influence of wind generated noise on the underwater soundscape is marginal.

The trajectory of the spectral level versus frequency in the 0.2–1 kHz range is modeled by a linear relation in a logarithmic frequency scale (dashed lines in Fig. 7)

$$\mathrm{SPL}(f) = s\,\log_{10} f + o, \tag{3}$$

where f is the frequency, s and o are the model coefficients, and SPL is the spectral level averaged over one-third octave bands (median averaging is used to remove outliers). The slopes $s_{0.2-1\mathrm{kHz}}$ (the subscript indicates the frequency range) in dB/dec for all rain rate and wind speed categories are listed in Fig. 8(a). Values that are computed from less than ten PSD samples are marked by an asterisk and should be treated with greater caution as they might not accurately represent the behavior of noise during rain. For rain rates below 10 mm/h and wind speeds below 4 m/s, slopes are between −8.2 and −6.1 dB/dec for the deep hydrophone and −4.9 and −3.6 dB/dec for the shallow hydrophone. As the rain rate or wind speed increases, $s_{0.2-1\mathrm{kHz}}$ increases at both locations.

For the deep hydrophone, slopes as high as −2 dB/dec are observed (rain rate 10–20 mm/h and wind speed 10–12 m/s; or rain rate 5–10 mm/h and wind speed >14 m/s). Although there is a strong indication that the slope further increases with increasing rain rate or increasing wind speed, more samples in those categories are needed to draw such a conclusion. For the shallow hydrophone, $s_{0.2-1\mathrm{kHz}}$ becomes positive as the rain rate or wind speed increases. The transition from negative to positive slopes is shown by a diagonal line in Fig. 8(a). All of the slopes above this line are negative, whereas the majority of slopes below this line are positive. This pattern is only violated in the >14 m/s wind speed category, where the slopes show somewhat smaller values than expected.

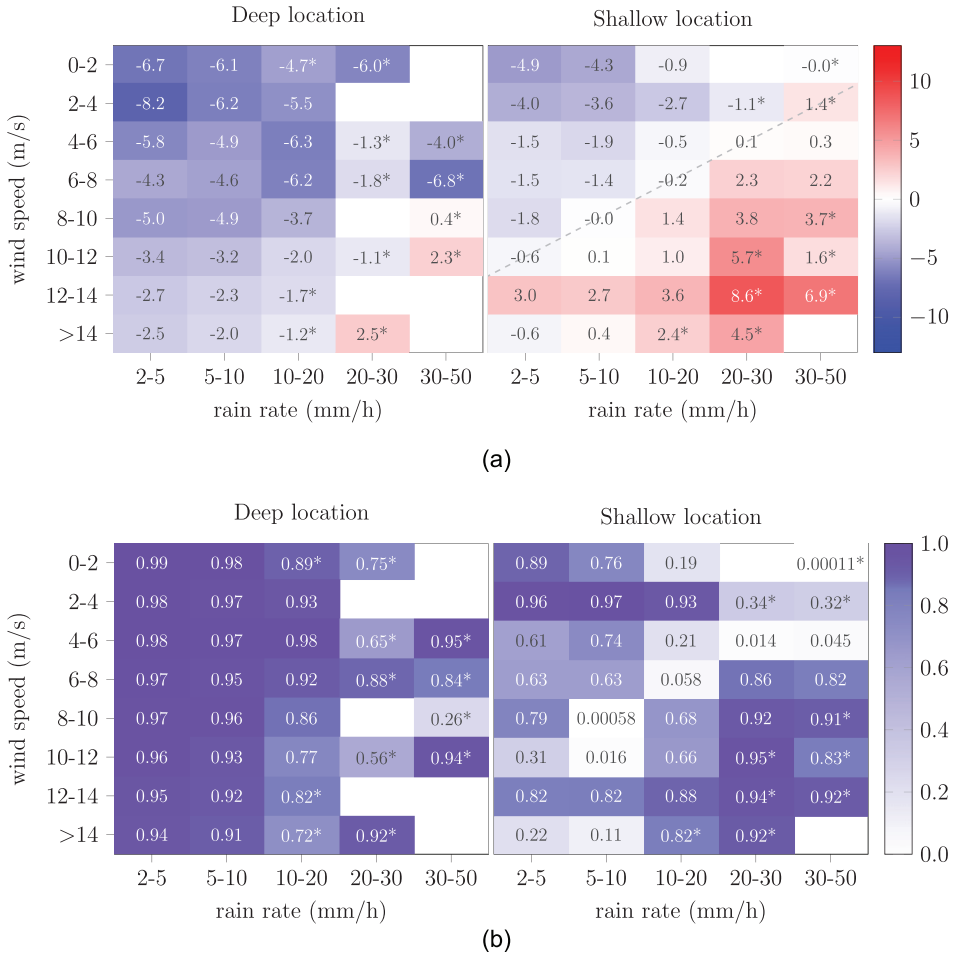

FIG. 8. (Color online) (a) Slopes $s_{0.2-1\text{kHz}}$ in dB/dec and (b) R^2 scores of the low frequency range linear regression. Whereas the deep hydrophone shows mainly negative slopes, a transition from negative to positive slopes can be observed for the shallow location. The dashed line on the right-hand side of (a) marks where the sign of the shallow location slope changes. R^2 scores indicate a strong linear relation for the deep location and a slightly weaker linear relation for the shallow location. Values that are computed from less than ten PSD samples are marked by an asterisk.

The coefficient of determination, denoted by R^2, is used as a metric for evaluating the performance of the regression model. Figure 8(b) shows the R^2 scores of the low frequency linear regression for both shallow and deep hydrophones. (R^2 scores are computed using the average spectral levels, thus, often resulting in values closer to one.) The deep hydrophone shows high R^2 scores for rain rates below 10 mm/h, therefore, favoring a linear model for those rain rate categories. Lower R^2 scores for rain rates above 10 mm/h are mainly due to a smaller number of PSD samples and, thus, a larger variability in the average PSDs. The greatest model mismatch can be observed at frequencies around 1 kHz, where the spectral levels seem to plateau as seen in the left plots of Fig. 7. Overall, a linear model seems to be a good fit to the average PSDs at the low frequency range for the data recorded at the deep hydrophone. The shallow hydrophone generally shows lower R^2 scores than the deep hydrophone. In the categories in which the slope is close to 0, R^2 values are low because the mean predicts the spectral levels well and, hence, the linear regression model does not improve the prediction. In the categories in which the slope significantly deviates from 0, R^2 values closer to one are observed.

C. Medium frequency range (1–10 kHz)

Similar to the low frequency range, the spectral level for frequencies between 1 and 10 kHz highly depends on the prevailing wind speed. For rain rates below 10 mm/h, the spectral level at adjacent wind speed bins typically differs by 2–3.5 dB at the deep location and 1.5–3.5 dB at the shallow location. As for the low frequency range, the spectral level versus $\log f$ relation for frequencies between 1 and 10 kHz is modeled according to Eq. (3). In this frequency range, however, spectral levels are averaged over one-sixth octave bands instead of one-third octave bands to have a larger number of bands for the regression. The slopes $s_{1-10\text{kHz}}$ and R^2 values for the 1–10 kHz regression model are listed in Fig. 9.

The spectral levels in this frequency range decrease faster compared to those at the low frequency range at both locations. The largest decrease is at low rain rates and high wind speeds. The slope becomes more gradual as the rain rate increases or the wind speed decreases. In general, both hydrophones show a similar pattern. However, the absolute values of the slopes at the deep location tend to be slightly larger for most rain rates and wind speeds.

The high R^2 values indicate a strong linear relation for wind speeds below 12 m/s and rain rates below 20 mm/h. Slightly higher R^2 values are observed at the shallow hydrophone. Comparing the trajectories of the spectral levels in the 1–10 kHz range between the deep and shallow hydrophones in Fig. 7 shows that the deep hydrophone exhibits ripples with small local maxima at 3 kHz and 9 kHz, which likely cause a slight drop in the R^2 scores. Whereas those

https://doi.org/10.1121/10.0005440

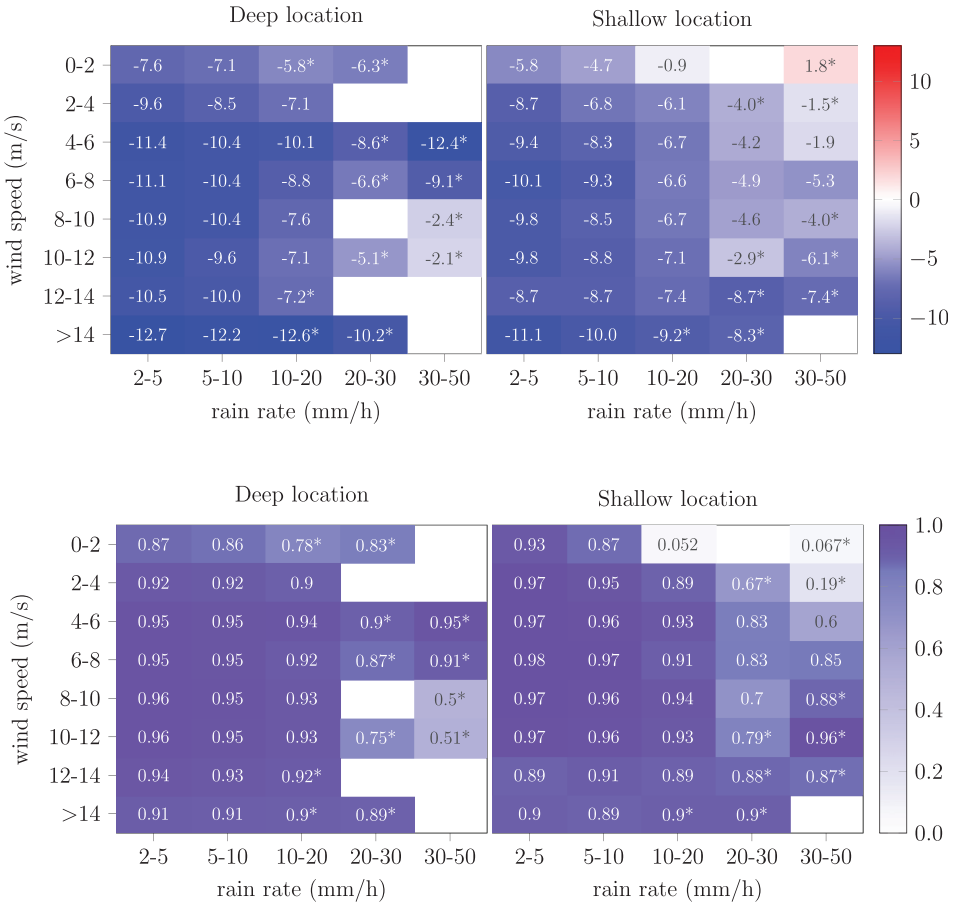

FIG. 9. (Color online) (a) Slopes $s_{1-10\text{kHz}}$ in dB/dec and (b) R^2 scores of the medium frequency range linear regression. Steeper slopes compared to the low frequency range can be observed for both locations. The R^2 scores indicate a strong linear relation for wind speeds below 12 m/s. Values that are computed from less than ten PSD samples are marked by an asterisk.

ripples are also observed in some PSDs at the shallow hydrophone, their shapes are less pronounced. At wind speeds greater than 12 m/s and rain rates above 20 mm/h, the relation between the spectral levels and frequency becomes more nonlinear and, hence, the R^2 scores decrease.

Some unusual behavior can be observed in this frequency range. (1) At the shallow hydrophone, there are small spikes between 1 and 2 kHz in most spectra, which are most likely caused by the electronic devices co-located with the hydrophone. (2) At the shallow hydrophone, there is a very high spectral level around 3 kHz in the 30–50 mm/h rain rate and 0–2 m/s wind speed category. This behavior might be explained by a hailstorm because the spectral shape matches the pattern of hail reported by Scrimger *et al.* (1987).

D. High frequency range (10–25 kHz)

The spectral levels for frequencies between 10 and 25 kHz are shown in Fig. 10. Note that in contrast to Fig. 7, each plot in Fig. 10 shows the spectral level for a fixed wind speed and various rain rates. At wind speeds below 4 m/s, the spectral levels for light rain and drizzle (rain rates below 10 mm/h) are dominated by a peak at around 15 kHz, caused by the damped oscillations of microbubbles. These peaks were previously reported by Bom (1969), Laville *et al.* (1991), Ma *et al.* (2005), Nystuen (1986), and Scrimger *et al.* (1987). During low wind speeds, the peak can even be observed for rain rates above 10 mm/h, indicating that a significant amount of small raindrops is still present during higher rain rates. At higher wind speeds, the spectral levels at all frequencies are significantly increased and cover the peaks. An apparent difference between the deep and shallow location is the smoothness of the spectral level. Although the deep hydrophone shows many local maxima and minima, the curves for the shallow hydrophone are much smoother.

The main challenge in modeling the high frequency range is to find a model that is flexible enough to show the highly nonlinear relation of the power spectra but still allows for some interpretability. We propose the following nonlinear equation, which is inspired by the five-coefficient model by Ma *et al.* (2005),

$$\text{SPL}_{10-25\text{kHz}} = \frac{A}{\left(1+\left(\frac{f}{f_{c,h}}\right)^{s_h}\right)\left(1+\left(\frac{f}{f_{c,l}}\right)^{s_l}\right)}, \quad (4)$$

where $\text{SPL}_{10-25\text{kHz}}$ is the spectral level between 10 and 25 kHz, averaged over one-twelfth octave bands (median averaging is used to remove outliers), A is the amplitude, $f_{c,h}$ is the high cutoff frequency, $f_{c,l}$ is the low cutoff frequency, s_h is the high frequency slope, and s_l is the low frequency

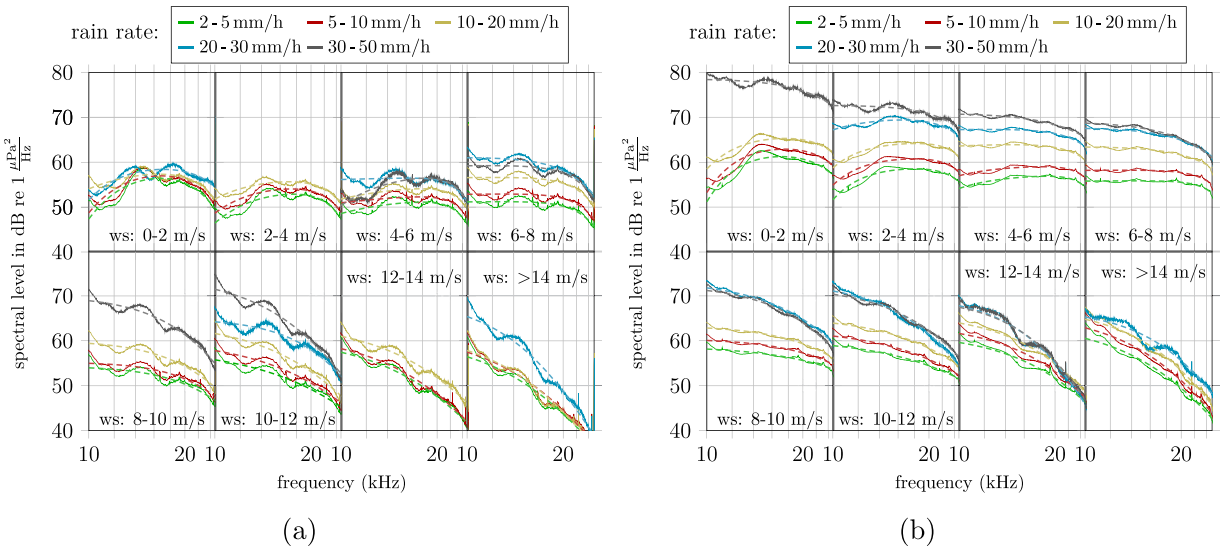

FIG. 10. (Color online) Average PSD estimates of rain induced noise at the (a) deep and (b) shallow locations for frequencies between 10 and 25 kHz (logarithmic frequency scale). The dashed lines show the regression curves according to Eq. (4). The high frequency range is dominated by a spectral peak at 15 kHz for wind speeds below 4 m/s. For high wind speeds, a steeply decreasing spectral level over frequencies can be observed.

slope. This model can be viewed as the concatenation of a Butterworth low pass filter with cutoff frequency $f_{c,h}$ and slope s_h and a Butterworth high pass filter with cutoff frequency $f_{c,l}$ and slope s_l. To ensure numerical stability during the optimization procedure, A is first set to one and the remaining model coefficients are determined using normalized spectral levels. Then, A is determined using linear least squares. We used the SciPy function *scipy.optimize.curve_fit* to perform the optimization (Virtanen *et al.*, 2020). The model coefficients are given in Table II for both locations, and the regression curves are shown as dashed lines in Fig. 10.

Although the model coefficients are determined empirically and their physical meaning may be limited, we still want to make a few statements on how the coefficients reflect the behavior observable in Fig. 10. (1) The amplitude A increases as the spectral level increases. (2) The high cutoff frequency $f_{c,h}$ is larger for the shallow location, whereas the high frequency slope s_h shows similar absolute values for both hydrophones. This causes the spectral level above 20 kHz to decrease more slowly for the shallow hydrophone compared to the deep hydrophone—a pattern that can also be observed in Fig. 10. (3) If a strong bandpass behavior can be observed in Fig. 10, the low cutoff frequency $f_{c,l}$ takes on values around 7 kHz and the low frequency slopes s_l have values on the order of -4 to -6. If no low frequency cutoff can be observed, $f_{c,l}$ assumes smaller values, and the slope is around zero for most wind speeds between 6 and 10 m/s or well below -10 for most wind speeds above 10 m/s.

E. Summary spectra

To highlight the rain rate dependency of noise during rain, we computed the summary spectra for each location based on the PSD estimates in Fig. 7. The results, along with the linear regression lines (dashed), are shown in Fig. 11. The spectra are obtained by averaging over all wind speed categories for a specific rain rate bin. Furthermore, the regression results from Ma *et al.* (2005) (triangle lines) in the 1–10 kHz range obtained for the tropical Pacific Ocean are plotted for comparison. The main observation is that the spectral level increases with increasing rain rate in both the 0.2–1 kHz and 1–10 kHz frequency range and at both locations. Furthermore, the difference in the spectral level between the lowest and highest rain rate categories increases with increasing frequency.

For frequencies between 0.2 and 1 kHz, spectral levels are slowly decreasing for increasing frequencies at the deep location. This decrease becomes more gradual as the rain rate increases. Spectral levels at the shallow hydrophone are almost constant in this frequency range for rain rates below 20 mm/h. For the two largest rain rate categories, however, a slight increase in the spectral level over frequencies can be observed. In the 1–10 kHz range, both the deep and shallow hydrophones show a decrease in the spectral level over frequencies. In this frequency range, the trajectory of the power spectra is very similar between both locations for rain rates below 20 mm/h. However, the average spectral levels are typically around 1–2 dB higher for the shallow hydrophone.

Compared to Ma's results, our northeast Pacific data at both locations show higher spectral levels and steeper slopes for all of the rain rate categories. This can likely be attributed to differences in the measurement location, water depth, and hydrophone deployment depth, but further research is necessary to confirm that.

F. Rain rate and wind speed dependence of noise spectral levels

To quantify the rain rate and wind speed dependence of the noise spectral level for various frequencies, the Pearson correlation coefficient between the spectral level and rain rate, as well as spectral levels and wind speed, is computed

https://doi.org/10.1121/10.0005440

TABLE II. Coefficients of high frequency nonlinear regression according to Eq. (4). $A, f_{c,h}, f_{c,l}, s_h$, and s_l are the amplitude, high cutoff frequency, low cutoff frequency, high frequency slope, and low frequency slope, respectively.

		Rain rate (mm/h)									
		Deep hydrophone					Shallow hydrophone				
	Wind speed (m/s)	2–5	5–10	10–20	20–30	30–50	2–5	5–10	10–20	20–30	30–50
A	0–2	58.71	58.91	59.16	59.78	—	62.62	64.08	66.40	—	79.85
	2–4	54.23	55.22	56.82	—	—	59.12	61.30	64.64	70.39	73.84
	4–6	52.38	53.70	55.31	58.62	58.06	57.36	59.41	64.62	68.17	71.85
	6–8	53.68	55.31	58.77	63.33	61.68	56.95	59.37	64.56	68.43	69.67
	8–10	56.78	57.73	62.12	—	71.40	59.59	61.39	63.97	73.41	72.53
	10–12	58.28	60.32	64.21	67.10	74.68	60.52	62.70	65.42	73.26	72.28
	12–14	60.81	61.57	64.07	—	—	61.78	63.81	66.10	70.08	69.63
	>14	60.89	61.90	62.40	69.63	—	64.09	66.33	67.57	67.21	—
$f_{c,l}$	0–2	7.30	7.08	4.35	6.72	—	7.62	7.41	6.52	—	0
	2–4	6.42	6.11	5.23	—	—	6.92	6.56	6.35	3.89	0
	4–6	3.39	1.26	3.04	0	5.55	4.41	3.99	0.49	0	0.32
	6–8	0	0	0	0	0	0	0	0	0	0
	8–10	0	0	0	—	0	0	0	0	0.95	0.75
	10–12	1.56	2.93	0.87	0	0.68	0.79	1.76	0.21	3.09	0.55
	12–14	1.80	1.56	0.80	—	—	0.34	1.13	0.50	3.64	2.72
	>14	0.97	2.15	1.09	2.96	—	1.49	1.67	1.16	3.18	—
s_l	0–2	−4.54	−4.54	−2.84	−4.64	—	−5.53	−5.33	−4.67	—	−0.20
	2–4	−4.03	−4.06	−3.60	—	—	−5.24	−5.10	−5.05	−3.24	−0.20
	4–6	−2.35	−1.41	−2.26	−0.35	−3.19	−3.45	−3.44	−1.38	−0.39	−0.20
	6–8	−0.14	−0.14	−0.15	−0.16	−0.15	−0.18	−0.18	−0.19	−0.21	−0.22
	8–10	−0.15	−0.14	−0.16	—	−0.19	−0.21	−0.20	−0.22	−26.24	−24.84
	10–12	−14.69	−23.96	−18.46	−0.16	−26.24	−24.47	−28.73	−28.48	−23.13	−27.23
	12–14	−14.46	−18.06	−25.12	—	—	−24.72	−24.94	−25.29	−28.04	−27.53
	>14	−18.81	−18.13	−18.34	−25.67	—	−15.21	−18.85	−27.15	−25.65	—
$f_{c,h}$	0–2	33.18	33.32	33.56	36.83	—	37.20	36.46	37.63	—	48.75
	2–4	31.67	32.32	33.37	—	—	34.14	33.91	33.06	37.77	44.21
	4–6	30.72	30.71	31.45	30.59	30.77	32.01	32.64	38.22	38.77	51.05
	6–8	33.13	32.89	33.33	36.05	33.34	34.69	36.21	44.92	44.15	44.53
	8–10	43.16	41.25	40.89	—	37.88	68.02	55.55	50.78	43.98	40.76
	10–12	45.79	42.96	39.30	37.91	35.44	58.54	51.77	48.13	37.16	40.69
	12–14	35.18	34.67	38.03	—	—	38.98	37.80	36.58	30.67	31.62
	>14	29.94	29.86	28.95	27.24	—	33.62	32.89	33.02	34.71	—
s_h	0–2	5.92	6.21	6.62	5.96	—	5.82	6.54	6.49	—	3.64
	2–4	8.17	7.90	7.42	—	—	8.73	9.02	10.07	6.43	4.43
	4–6	9.92	10.42	9.68	10.57	9.79	11.73	10.69	6.48	6.18	3.44
	6–8	7.40	7.63	7.09	4.91	6.66	8.98	7.62	4.24	3.92	3.49
	8–10	3.18	3.50	3.05	—	3.01	2.30	2.76	2.84	2.56	2.84
	10–12	2.04	2.16	2.32	3.24	2.46	2.04	2.20	2.40	2.66	2.57
	12–14	2.26	2.31	2.24	—	—	2.44	2.52	2.63	3.04	2.99
	>14	2.32	2.35	2.39	2.73	—	2.34	2.44	2.64	2.84	—

for all 2049 frequency bins between 0 and 32 kHz. The resulting frequency dependent correlation coefficients are median-averaged over one-third octave bands and shown in Fig. 12.

Figure 12(a) shows that the correlation between the spectral level and rain rate increases with frequency until it reaches a maximum of about 0.5 at the shallow location and 0.4 at the deep location at 13 kHz. The maximum correlation corresponds to the high frequency peak caused by the oscillation of microbubbles that are primarily generated by small rain drops during light rain and drizzle. This is less surprising as most of the data in this study were recorded for rain rates below 20 mm/h. On the other hand, the correlation between the spectral level and wind speed shown in Fig. 12(b) has a broad maximum between 0.5 and 1 kHz at the deep location and between 0.8 and 3 kHz at the shallow location. For frequencies above 10 kHz, a steep decrease in the correlation occurs at both locations. This implies that for frequencies around 13 kHz, the noise spectral level is essentially independent of the wind speed and only depends on the rain rate. This has important implications for tasks such as remote sensing of rain rates based on underwater acoustic recordings. If a simple conversion algorithm that relates the sound spectral level at a particular frequency to the prevailing rain

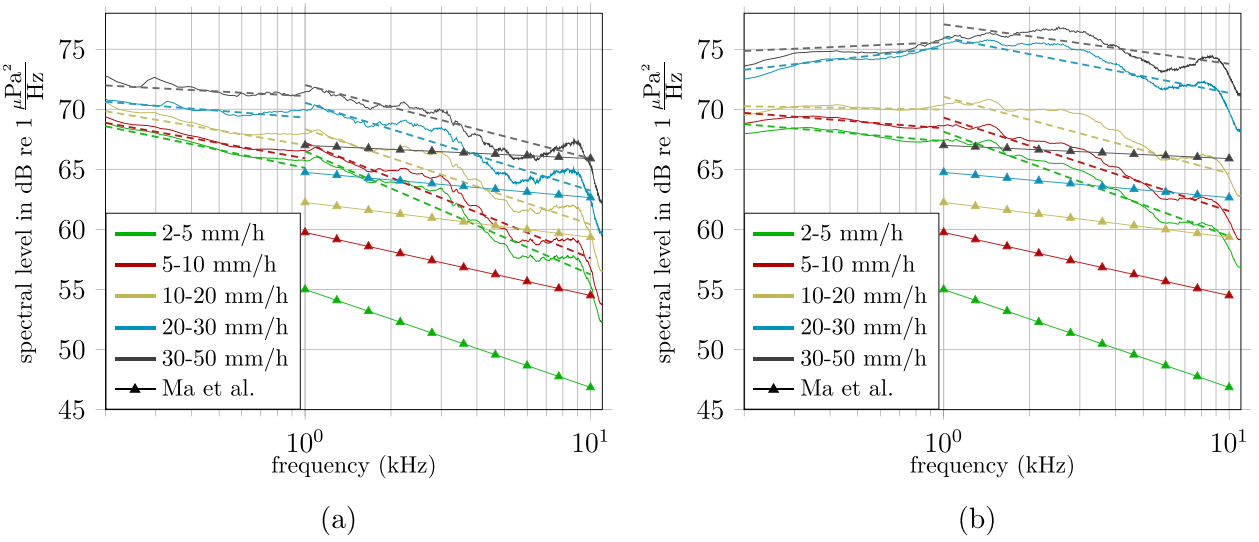

FIG. 11. (Color online) Summary spectra for the (a) deep and (b) shallow hydrophones. The dashed lines are obtained by linear regression of the summary spectra mapped into one-third octave bands (0.2–1 kHz frequency range) and one-sixth octave bands (1–10 kHz frequency range). The triangle lines are the linear regression results reported by Ma *et al.* (2005). Our summary spectra differ significantly in level and trajectory from the results reported by Ma.

rate is to be designed, the sound spectral level is desired to have a high correlation with the rain rate but a low correlation with the wind speed. Such an algorithm was developed by Ma and Nystuen (2005) for data from the tropical Pacific. The authors used an acoustic frequency of 5 kHz as their spectral levels at this frequency were highly dependent on the rain rate but approximately independent from the wind speed. For the northeast Pacific data in this study, a frequency of 13 kHz should be chosen instead. However, it is noted that Ma and Nystuen (2005) had more measurements for high rain rates (>20 mm/h), whereas most acoustic data in this study correspond to rain rates below 20 mm/h. Higher rain rates are associated with larger rain drops, whose impact and bubble sound can contribute significantly to frequencies below 10 kHz (Medwin *et al.*, 1992; Nystuen and Medwin, 1995; Pumphrey *et al.*, 1989). Therefore, spectral levels during heavy rain are likely to show a higher correlation for frequencies below 10 kHz.

An interesting phenomenon can be observed when comparing the correlation curves between both locations. On the one hand, the correlation between the spectral level and rain rate is significantly higher at the shallow location. This is consistent with results reported by Anagnostou *et al.* (2008), where the authors have shown that acoustic measurements from shallow hydrophones correlate better with radar rain rate measurements that are averaged over a smaller surface area. As the rain rate signals in this study are obtained by surface buoys, no spatial averaging of the rain rate measurements is performed. On the other hand, the correlation between the spectral level and wind speed is higher at the deep location. We speculate that the lower correlation for the shallow site is a result of the smaller effective surface listening area of the hydrophone and, therefore, lesser

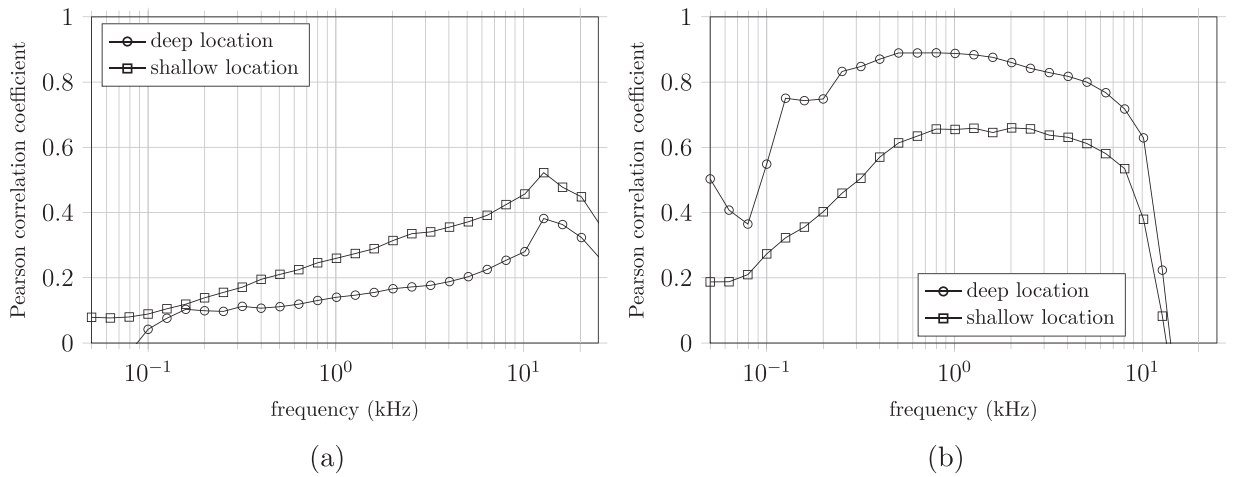

FIG. 12. The Pearson correlation between the (a) spectral level and rain rate and (b) spectral level and wind speeds. The correlation is computed for all 2049 frequency bins between 0 and 32 kHz before being median-averaged into one-third octave bands.

https://doi.org/10.1121/10.0005440

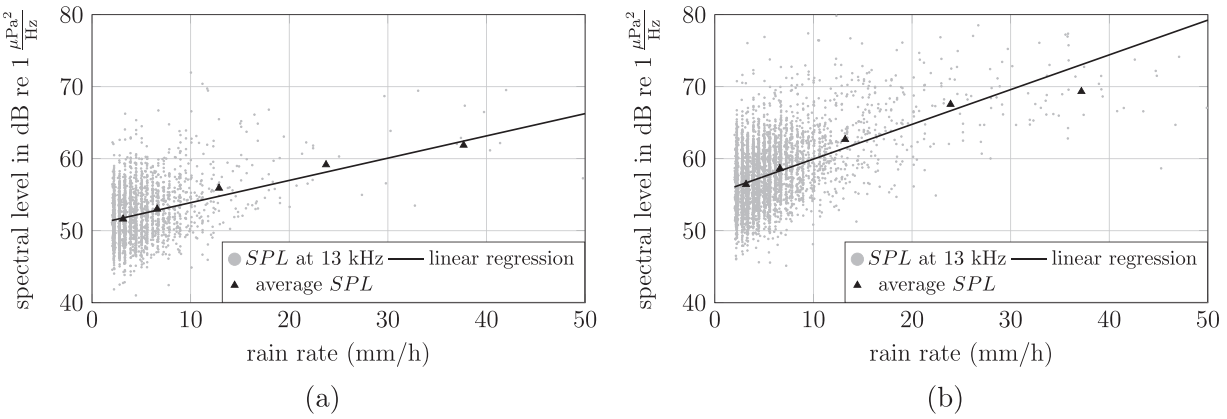

FIG. 13. The Spectral level (SPL) at 13 kHz versus the rain rate for the (a) deep and (b) shallow locations. The solid line is obtained by performing the linear regression on all of the data points. The triangles represent average spectral levels and average rain rates in their respective rain rate categories. Spectral levels are increasing with an average rate of 0.31 dB/mm h^{-1} for the deep location and 0.48 dB/mm h^{-1} for the shallow location.

spatial averaging of the acoustic signal (see Sec. III A). That is, single wave breaking events have a stronger effect on the sound levels received by the shallow hydrophone, resulting in a larger variability of the sound spectral levels for a given wind speed.

Scatter plots along with linear regression lines for the spectral level versus rain rate and spectral level versus wind speed relations at 13 kHz are shown in Figs. 13 and 14, respectively. The average spectral levels of all rain rate and wind speed categories are also computed and illustrated by triangles in each plot. For the spectral level versus rain rate plots in Fig. 13, a large variability in the data can be observed. Especially for low rainfall rates, spectral levels likely vary within a 20 dB range at both locations. Nonetheless, an overall increase in the spectral level of 0.31 dB/mm h^{-1} at the deep location and 0.48 dB/mm h^{-1} at the shallow location can be observed. The linear regression lines, in general, match well to the average spectral levels in each rain rate category. Only for rain rates above 30 mm/h, the model seems to overestimate the observed spectral levels. A possible explanation for this phenomenon is that the impact of small raindrops on the underwater sound field does not continue to increase with increasing rain rate, but instead the drop size distribution shifts to larger rain drops (Nystuen, 2001). This suggests that a nonlinear model may be necessary to model the spectral level versus rain rate relation over a wide range of rain rates. However, to draw more definite conclusions more data for high rain rates, as well as estimates of the drop size distribution, are necessary.

Figure 14 shows that the spectral level at 13 kHz is almost independent of the wind speed as predicted by the curves in Fig. 12. Only a slight increase in 0.22 dB/m s^{-1} for the deep location and 0.07 dB/m s^{-1} for the shallow location can be observed. Overall, the average spectral levels within each wind speed category (triangles) show good agreement with the regression lines. It is interesting to note that the average spectral levels, particularly, at the deep location show some weak oscillations with increasing wind speed. This can be explained as follows. For very low wind speeds (below 3 m/s), the average spectral level at 13 kHz is dominated by the sound from the oscillating microbubbles due to small rain drops (Medwin *et al.*, 1992). As the wind speed increases, the amount of microbubbles decreases

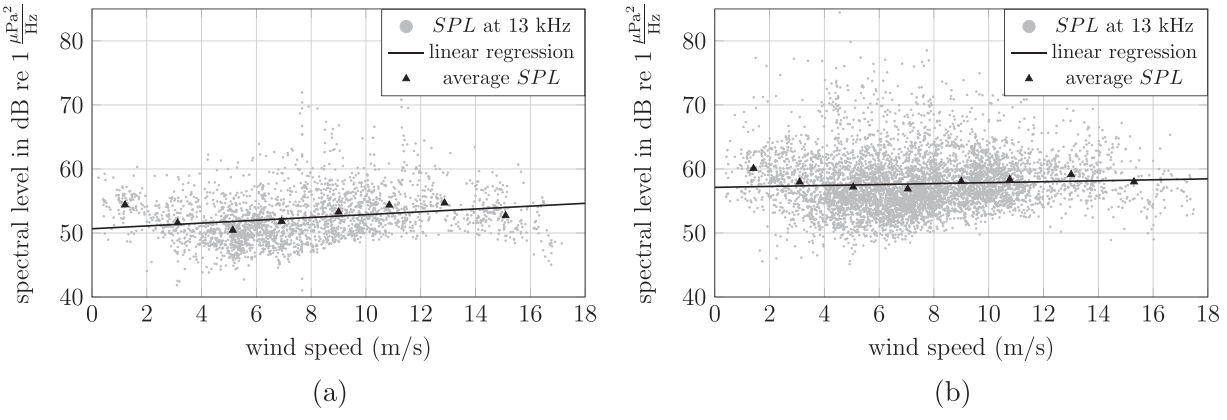

FIG. 14. The Spectral level (SPL) at 13 kHz versus the wind speed for the (a) deep and (b) shallow locations. The solid line is obtained by performing the linear regression on all of the data points. The triangles represent the average spectral levels and average wind speeds in their respective wind speed categories. As predicted by Fig. 12(b), the spectral levels are not significantly increasing with wind speed at this frequency.

significantly (Medwin *et al.*, 1990), whereas noise due to wind does not yet contribute notably to the spectral level. This causes the first minimum around 5–6 m/s. With further increasing wind speed, the noise level is increasingly dominated by the sound from breaking waves and whitecaps until it reaches a maximum at approximately 13 m/s. A further increase in the wind speed can have a negative effect on the sound propagation due to increased attenuation and scattering caused by a layer of air bubbles, which is generated by breaking waves (Farmer and Lemon, 1984). This bubble layer becomes wider and penetrates deeper into the ocean as the wind speed increases, thus, resulting in a stronger attenuation and, consequently, a decrease in the noise level at high wind speeds.

VI. CONCLUSIONS

We have evaluated acoustic and meteorological data recorded at two locations off the coast of Oregon between December 2015 and June 2019 to analyze noise during rain at the northeast Pacific continental margin. Linear and nonlinear models have been used to characterize the noise spectra in different frequency ranges. The results can be summarized as follows. (1) In contrast to previous measurements conducted by Ma *et al.* (2005), our noise spectral levels during rain show a strong wind speed dependency over a broad frequency range. (2) Between 0.2 and 1 kHz, the spectral levels show a slope of -8.2 to -2.0 dB/dec for the deep location and -4.9 to 3.8 dB/dec for the shallow location. For both sites, the slope increases with increasing wind speed or increasing rain rate. (3) Steeper slopes, typically between -6.0 and -12.0 dB/dec, can be observed in the 1–10 kHz range for both hydrophones. Here, the steepness increases with increasing wind speed and decreasing rain rate. (4) The 10–25 kHz range can be modeled using a five-coefficient nonlinear model to characterize the spectral peak around 15 kHz caused by light rain and drizzle.

We have further investigated the dependence of the spectral level on the rain rate as well as the dependence of the spectral level on the wind speed for various frequencies. We found that the highest correlation between the spectral level and rain rate occurs at approximately 13 kHz, thus, corresponding to the high frequency peak due to light rain and drizzle. At this frequency, spectral levels during rain increase with a rate of 0.31 dB/mm h^{-1} for the deep location and 0.48 dB/mm h^{-1} for the shallow location. We have also found that at 13 kHz, spectral levels are approximately independent of the wind speed if rain is present. For frequencies below 10 kHz, on the other hand, spectral levels are only weekly dependent on the rain rate but strongly dependent on the wind speed.

The results in this study can serve as a detailed statistical analysis of the spectral behavior of noise during rain at the northeast Pacific continental margin for rain rates below 20 mm/h. For higher rain rates, more data are needed to accurately characterize the noise level. Our results can also serve as a starting point for estimating rain rates and wind speeds from acoustic data. A respective algorithm for estimating rain rates, based on a simple conversion using spectral levels at 5 kHz, has been proposed by Ma and Nystuen (2005). However, our data clearly indicate that this algorithm would need to be adapted for other measurement sites.

ACKNOWLEDGMENTS

This research was supported by the Office of Naval Research Grant No. N00014-19-1-2644. The authors would like to thank Barry Ma for valuable discussions and suggestions at the beginning of this research effort.

[1]See www.geomapapp.org CC BY (Last viewed 6 June 2020).
[2]NFS OOI Data Portal, Broadband Acoustic Receiver (CE04OSBP-LJ01C-11-HYDBBA105) data from 1 December 2015 to 30 June 2019, available at https://ooinet.oceanobservatories.org (Last viewed 6 June 2020).
[3]NFS OOI Data Portal, Bulk Meteorology Instrument Package (CE04OSSM-SBD11-06-METBKA000) data from 1 December 2015 to 30 June 2019, available at https://ooinet.oceanobservatories.org (Last viewed 6 June 2020).
[4]NFS OOI Data Portal, Broadband Acoustic Receiver (CE02SHBP-LJ01D-11-HYDBBA106) data from 01 December 2015 to 30 June 2019, available at https://ooinet.oceanobservatories.org (Last viewed 6 June 2020).
[5]NFS OOI Data Portal, Bulk Meteorology Instrument Package (CE02SHSM-SBD11-06-METBKA000) data from 01 December 2015 to 30 June 2019, available at https://ooinet.oceanobservatories.org (Last viewed 7 June 2020).
[6]NFS OOI Data Portal, CTD (shallow location, surface buoy CTD—CE02SHSM-RID27-03-CTDBPC000, shallow profiler, CE02SHSP-SP001-08-CTDPFJ000, hydrophone CTD—CE02SHBP-LJ01D-06-CTDBPN106; deep location, surface buoy CTD—CE04OSSM-RID27-03-CTDBPC000, shallow profiler—CE04OSPS-SF01B-2A-CTDPFA107, 200 m platform—CE04OSPS-PC01B-4A-CTDPFA109, deep profiler—CE04OSPD-DP01B-01-CTDPFL105, hydrophone CTD—CE04OSBP-LJ01C-06-CTDBPO108) data from 1 September 2015 to 31 December 2019, available at https://ooinet.oceanobservatories.org (Last viewed 7 June 2020).

Anagnostou, M. N., Nystuen, J. A., Anagnostou, E. N., Nikolopoulos, E. I., and Amitai, E. (**2008**). "Evaluation of underwater rainfall measurements during the ionian sea rainfall experiment," IEEE Trans. Geosci. Remote Sens. **46**(10), 2936–2946.
Anderson, V. C. (**1979**). "Variation of the vertical directionality of noise with depth in the north pacific," J. Acoust. Soc. Am. **66**(5), 1446–1452.
Bannister, R. W. (**1986**). "Deep sound channel noise from high-latitude winds," J. Acoust. Soc. Am. **79**(1), 41–48.
Barclay, D. R., and Buckingham, M. J. (**2013**). "The depth-dependence of rain noise in the philippine sea," J. Acoust. Soc. Am. **133**(5), 2576–2585.
Berger, J., Bidlot, J.-R., Dzieciuch, M. A., Farrell, W. E., Worcester, P. F., and Stephen, R. A. (**2018**). "A deep ocean acoustic noise floor, 1–800 hz," J. Acoust. Soc. Am. **143**(2), 1223–1233.
Bom, N. (**1969**). "Effect of rain on underwater noise level," J. Acoust. Soc. Am. **45**(1), 150–156.
Chen, C., and Millero, F. J. (**1977**). "Speed of sound in seawater at high pressures," J. Acoust. Soc. Am. **62**(5), 1129–1135.
Farmer, D. M., and Lemon, D. D. (**1984**). "The influence of bubbles on ambient noise in the ocean at high wind speeds," J. Phys. Oceanogr. **14**(11), 1762–1778.
Farrokhrooz, M., Wage, K. E., Dzieciuch, M. A., and Worcester, P. F. (**2017**). "Vertical line array measurements of ambient noise in the North Pacific," J. Acoust. Soc. Am. **141**(3), 1571–1581.
Franz, G. J. (**1959**). "Splashes as sources of sound in liquids," J. Acoust. Soc. Am. **31**(8), 1080–1096.
Kerman, B. R. (**1984**). "Underwater sound generation by breaking wind waves," J. Acoust. Soc. Am. **75**(1), 149–165.

Knudsen, V. O., Alford, R. S., and Emling, J. W. (**1948**). "Underwater ambient noise," J. Mar. Res. **7**(3), 410–429.
Laville, F., Abbott, G. D., and Miller, M. J. (**1991**). "Underwater sound generation by rainfall," J. Acoust. Soc. Am. **89**(2), 715–721.
Lemon, D. D., Farmer, D. M., and Watts, D. R. (**1984**). "Acoustic measurements of wind speed and precipitation over a continental shelf," J. Geophys. Res.: Oceans **89**(C3), 3462–3472, https://doi.org/10.1029/JC089iC03p03462.
Ma, B. B., and Nystuen, J. A. (**2005**). "Passive acoustic detection and measurement of rainfall at sea," J. Atmos. Ocean. Technol. **22**(8), 1225–1248.
Ma, B. B., Nystuen, J. A., and Lien, R.-C. (**2005**). "Prediction of underwater sound levels from rain and wind," J. Acoust. Soc. Am. **117**(6), 3555–3565.
McKenna, M. F., Ross, D., Wiggins, S. M., and Hildebrand, J. A. (**2012**). "Underwater radiated noise from modern commercial ships," J. Acoust. Soc. Am. **131**(1), 92–103.
Medwin, H., Kurgan, A., and Nystuen, J. A. (**1990**). "Impact and bubble sound from raindrops at normal and oblique incidence," J. Acoust. Soc. Am. **88**(1), 413–418.
Medwin, H., Nystuen, J. A., Jacobus, P. W., Ostwald, L. H., and Snyder, D. E. (**1992**). "The anatomy of underwater rain noise," J. Acoust. Soc. Am. **92**(3), 1613–1623.
Monahan, E. C. (**1971**). "Oceanic whitecaps," J. Phys. Oceanogr. **1**(2), 139–144.
Monahan, E. C., and Lu, M. (**1990**). "Acoustically relevant bubble assemblages and their dependence on meteorological parameters," IEEE J. Ocean. Eng. **15**(4), 340–349.
Nystuen, J. A. (**1986**). "Rainfall measurements using underwater ambient noise," J. Acoust. Soc. Am. **79**(4), 972–982.
Nystuen, J. A. (**1996**). "Acoustical rainfall analysis: Rainfall drop size distribution using the underwater sound field," J. Atmos. Ocean. Technol. **13**(1), 74–84.
Nystuen, J. A. (**1999**). "Relative performance of automatic rain gauges under different rainfall conditions," J. Atmos. Ocean. Technol. **16**(8), 1025–1043.
Nystuen, J. A. (**2001**). "Listening to raindrops from underwater: An acoustic disdrometer," J. Atmos. Ocean. Technol. **18**(10), 1640–1657.
Nystuen, J. A., McGlothin, C. C., and Cook, M. S. (**1993**). "The underwater sound generated by heavy rainfall," J. Acoust. Soc. Am. **93**(6), 3169–3177.
Nystuen, J. A., and Medwin, H. (**1995**). "Underwater sound produced by rainfall: Secondary splashes of aerosols," J. Acoust. Soc. Am. **97**(3), 1606–1613.
Nystuen, J. A., Proni, J. R., Black, P. G., and Wilkerson, J. C. (**1996**). "A comparison of automatic rain gauges," J. Atmos. Ocean. Technol. **13**(1), 62–73.
Parks, S. E., Urazghildiiev, I., and Clark, C. W. (**2009**). "Variability in ambient noise levels and call parameters of north atlantic right whales in three habitat areas," J. Acoust. Soc. Am. **125**(2), 1230–1239.
Pumphrey, H. C., Crum, L. A., and Bjørnø, L. (**1989**). "Underwater sound produced by individual drop impacts and rainfall," J. Acoust. Soc. Am. **85**(4), 1518–1526.
Ryan, W. B. F., Carbotte, S. M., Coplan, J. O., O'Hara, S., Melkonian, A., Arko, R., Weissel, R. A., Ferrini, V., Goodwillie, A., Nitsche, F., Bonczkowski, J., and Zemsky, R. (**2009**). "Global multi-resolution topography (GMRT) synthesis data set," Geochem., Geophys., Geosyst. **10**(3), Q03014, https://doi.org/10.1029/2008GC002332.
Schwock, F., and Abadi, S. (**2021**). "Statistical properties of a modified welch method that uses sample percentiles," in *Proceedings of the 2021 IEEE International Conference on Acoustics, Speech and Signal Processing (ICASSP)*, June 6–11, Toronto, Canada, pp. 5165–5169.
Schwock, F., Ragland, J., Munson, M., and Abadi, S. (**2020**). "OOIPy: A Python toolbox designed to aid in the scientific analysis of Ocean Observatories Initiative (OOI) data," doi: 10.5281/zenodo.4276862.
Scrimger, J. A., Evans, D. J., McBean, G. A., Farmer, D. M., and Kerman, B. R. (**1987**). "Underwater noise due to rain, hail, and snow," J. Acoust. Soc. Am. **81**(1), 79–86.
Scrimger, J. A., Evans, D. J., and Yee, W. (**1989**). "Underwater noise due to rain—Open ocean measurements," J. Acoust. Soc. Am. **85**(2), 726–731.
Vagle, S., Large, W. G., and Farmer, D. M. (**1990**). "An evaluation of the wotan technique of inferring oceanic winds from underwater ambient sound," J. Atmos. Ocean. Technol. **7**(4), 576–595.
Virtanen, P., Gommers, R., Oliphant, T. E., Haberland, M., Reddy, T., Cournapeau, D., Burovski, E., Peterson, P., Weckesser, W., Bright, J., van der Walt, S. J., Brett, M., Wilson, J., Millman, K. J., Mayorov, N., Nelson, A. R. J., Jones, E., Kern, R., Larson, E., Carey, C. J., Polat, İ., Feng, Y., Moore, E. W., VanderPlas, J., Laxalde, D., Perktold, J., Cimrman, R., Henriksen, I., Quintero, E. A., Harris, C. R., Archibald, A. M., Ribeiro, A. H., Pedregosa, F., and van Mulbregt, P., and SciPy 1.0 Contributors. (**2020**). "SciPy 1.0: Fundamental algorithms for scientific computing in Python," Nat. Methods **17**, 261–272.
Wagstaff, R. A. (**1981**). "Low-frequency ambient noise in the deep sound channel—The missing component," J. Acoust. Soc. Am. **69**(4), 1009–1014.
Welch, P. (**1967**). "The use of fast Fourier transform for the estimation of power spectra: A method based on time averaging over short, modified periodograms," IEEE Trans. Audio Electroacoust. **15**(2), 70–73.
Wenz, G. M. (**1962**). "Acoustic ambient noise in the ocean: Spectra and sources," J. Acoust. Soc. Am. **34**(12), 1936–1956.